Chemosphere 365 (2024) 143371

Contents lists available at ScienceDirect

Chemosphere

journal homepage: www.elsevier.com/locate/chemosphere

Performance and analysis of kappa-carrageenan hydrogel for PFOA-contaminated soil remediation wastewater treatment

Lilyan Alsaka [a], Ibrar Ibrar [a], Ali Altaee [a,*], John Zhou [a], Mahedy Hasan Chowdhury [a], Maryam AL-Ejji [b], Alaa H. Hawari [c]

[a] Centre for Green Technology, School of Civil and Environmental Engineering, University of Technology Sydney, 15 Broadway, NSW, 2007, Australia
[b] Center of Advanced Materials, Qatar University, PO Box 2713, Doha, Qatar
[c] Department of Civil and Environmental Engineering, College of Engineering, Qatar University, PO Box 2713, Doha, Qatar

HIGHLIGHTS

- AC and vanillin kC were fabricated for PFOA wastewater treatment.
- The 2 cm thickness 3%kC-AC and 3%kC-V hydrogels achieved 25.6 and 21.5 LMH water flux.
- 3%kC-AC hydrogel rejected 86.9% PFOA compared to 81% rejection for the 3%kC-AC hydrogel.
- 3%kC-AC hydrogel rejected 99% of Al, 75% Si, 83% of Cl, 76% of Na, 90% of K and 96.5% of Turbidity.

GRAPHICAL ABSTRACT

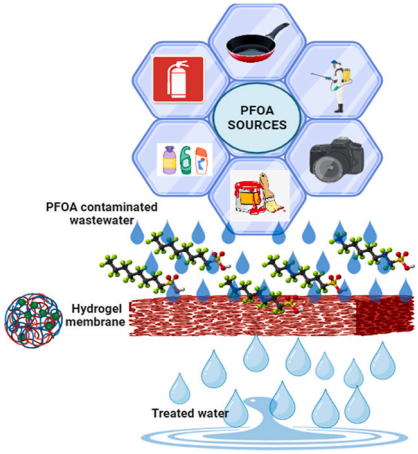

ARTICLE INFO

Handling editor: HEESOO EUN

Keywords:
Hydrogel membranes
Filtration
PFOA
Kappa-carrageenan
Wastewater

ABSTRACT

Perfluorooctanoic acid is an emerging pollutant with exceptional resistance to degradation and detrimental environmental and health impacts. Conventional physical and chemical processes for Perfluorooctanoic acid are either expensive or inefficient. This study developed an environmentally sustainable and cost-effective gravity-driven kappa-carrageenan (kC)-based hydrogel for perfluorooctanoic acid (PFOA) removal from synthetic and actual wastewater. Two kC filters were prepared by mixing activated carbon (AC) or vanillin (V) with the kC hydrogel to optimize the hydrogel selectivity and water permeability. Experimental work revealed that the PFOA rejection and water permeability increased with the AC and V concentrations in the kC hydrogel. Experiments also evaluated the impact of feed pH, PFOA concentration, hydrogel composition, and hydrogel thickness on its performance. Due to pore size shrinkage, the AC-kC and V-kC hydrogels achieved the highest PFOA rejection at pH 4, whereas the water flux decreased. Increasing the PFOA concentration reduced water flux and increased PFOA rejection. For 2 cm hydrogel thickness, the water flux of 3%kC-0.3%AC and 3%kC-3%V hydrogels was

* Corresponding author.
E-mail address: ali.altaee@uts.edu.au (A. Altaee).

https://doi.org/10.1016/j.chemosphere.2024.143371
Received 15 February 2024; Received in revised form 8 August 2024; Accepted 18 September 2024
Available online 19 September 2024

25.6 LMH and 21.5 LMH, and the corresponding PFOA rejection was 86.9% for 3%kC-0.3%AC and 85.7% for 3% kC-3%V. Finally, the kC-0.3%AC hydrogel removed 81.1% of PFOA from wastewater of 179 mg/L initial concentration compared to 79.3% for the kC-3%V hydrogel. After three filtration cycles, the water flux decline of 3% kC-0.3%AC was less than 10%. The gravity dead-end kC hydrogel provides sustainable PFOA wastewater treatment with biodegradable and natural materials.

1. Introduction

Polyfluoroalkyl substances (PFAS) are synthetic compounds widely utilized for their water and grease resistance and thermal stability in diverse industrial and consumer applications. Characterized by robust fluorine-carbon bonds, PFAS exhibit exceptional chemical stability, contributing to their persistence in the environment. PFAS are categorized into perfluoroalkyl sulfonates (PFAS) and perfluoroalkyl carboxylates (PFCA). Despite their versatility, PFAS have raised environmental concerns due to their pervasive presence and potential adverse effects on human health and ecosystems globally. Consequently, developing effective PFOA removal strategies has become an area of intense research and innovation (Buck et al., 2011; Milley et al., 2018; Zheng et al., 2017). PFOA, typically found at low concentrations, is treated by one of these methods: adsorption, ion exchange, or membrane filtration (Appleman et al., 2014). Adsorbents used for PFAS treatment include activated carbon (AC), silica, zeolites, aminated rice husk, g-C_3N_4, MOFs, COFs, and modified chitosan(Lei, 2023). PFAS adsorption relies on electrostatic and hydrophobic forces influenced by molecular structure and physicochemical properties. Solution pH, regeneration costs, and ionic strength affect the adsorption broad application for PFAS treatment. Also, short-chain PFAS (<C6) presents difficulties for conventional adsorbers like AC (Das and Ronen, 2022).

Several studies recommended nanofiltration (NF) and reverse osmosis (RO) for PFAS treatment, knowing that RO outperforms NF membranes for PFAS rejection. RO membranes consistently exhibit rejection rates of over 99% for multiple PFAS species, including PFOS, PFHxA, PFOA, and PFDA (Tang et al., 2006; Zeng et al., 2017a,b,c), in contrast to approximately 95% rejection observed with NF membranes (Franke et al., 2019; Tang et al., 2006). In a study by (Flores et al., 2013), RO effectively removed over 99% of fluorinated compounds (PFOA and PFOS) from wastewater, resulting in trace concentrations (PFOA <4.2–5.5 ng/L, PFOS 3–21 ng/L) below the US-recommended limit for drinking water (70 ng/L). However, it is crucial to note that while membrane technologies, particularly RO, are highly effective, they pose economic challenges, and handling residual PFAS concentrate remains problematic.

Recent focus has been on innovative hydrogel substances derived from natural and synthetic polymer sorbents for addressing PFAS contamination in aqueous environments. The adsorption of PFOA to chitosan and ethylene glycol exhibits a maximum capacity adsorption of 1275.9 mg/g, rendering them attractive adsorbents for PFOA removal from wastewater (Long et al., 2019). For example, hydrogel based on poly(acrylamide) with incorporated powdered AC demonstrated removal efficiencies of up to 98% for perfluorooctanoic sulfonic acid (PFOS) and 96% for perfluorooctanoic acid (PFOA) (Klaus et al., 2023). Ateia et al. reported the functionalized cellulose achieved a rapid 70–80% removal of PFOA and PFOS within the first 100 s (Ateia et al., 2019). Researchers enhanced PFAS affinity by incorporating ionic fluorogels through thermally initiated radical copolymerization of perfluoropolyethers PFPE with methacrylate chain-end functionality (Fluorolink MD 700) and an amine-containing monomer (2-dimethylaminoethyl methacrylate, DMAEMA). This approach achieved >95% removal of diverse PFAS, including PFOA and PFOS, from wastewater treatment plant samples (Kumarasamy et al., 2020). Chitosan, a polysaccharide containing amine groups, manifests adsorptive properties concerning PFAS through ionic interactions involving the carboxylic/sulfonic groups of PFAS and the cationic groups inherent in the polymer (Zhang et al., 2011). Crosslinking with epoxy epichlorohydrin (ECH) enhances affinity, forming a molecularly imprinted hydrogel that adsorbs over 50% of PFAS, even in competing pollutants (Yu et al., 2008).

Kappa-carrageenan (kC) is another polysaccharide widely used in adsorption and membrane filtration. It has a robust gel-forming capacity due to its helicoidal shape, which plays a crucial role in gelation (Liu and Li, 2016). Ibrar and co-workers developed a kC-vanillin hydrogel filter for landfill leachate wastewater treatment, which achieved a 27 LMH water flux, 77% rejection of organic carbon (TOC), and 95% for color removal (Ibrar et al., 2023). Esmaeili et al. (2020) enhanced polyethersulfone (PES) membrane hydrophilicity and antifouling properties by incorporating 6 wt% vanillin, resulting in a 40% increase in water flux compared to the control (Esmaeili et al., 2020). The study examined the influence of kC content in PVDF/kC composite membranes and found that 1.0 wt% of kCg significantly improved membrane properties, enhancing characteristics and increasing dye rejection and water permeance (Alam et al., 2019). Yadav et al. (2022) enhanced a nanofiltration (NF) membrane with a kC-GO solution for leachate wastewater treatment, achieving a 95.73% water flux recovery and reduced fouling compared to the uncoated NF membrane.

Although kC was investigated for wastewater treatment, studies on kC applications for PFAS removal from wastewater are scarce. kC, with excellent characteristics, such as plenty of functional groups, high adsorption capacity, biodegradable, thermal stability, outstanding mechanical strength, and exceptional gelling mechanisms, would be suitable for treatment from organic and inorganic pollutants (Ibrar et al., 2023). This study has developed novel gravity-driven kC-based hydrogel filters that operate in dead-end mode for PFOA removal from aqueous solutions. The dead-end filtration mode will facilitate hydrogel recovery at the end of the filtration process. The kC hydrogels were mixed with AC and vanillin (V) nanoparticles to improve their adsorption capacity. Two hydrogel filters, kC-vanillin (kC-V) and kC-AC, were investigated for PFOA treatment. kC-V, already used for ions removal from leachate wastewater, will be tested for PFOA removal. Vanillin was used as a crosslinker and pore-forming agent to enhance the hydrophilicity and water permeability of the hydrogel. Besides, the kC-AC hydrogel filter was investigated for the first time for PFOA treatment. Adding AC to hydrogel improved the hydrogel water permeability and adsorption capacity. A parametric study evaluated the impact of feed concentration, hydrogel thickness, and feed pH on PFOA removal. The research questions for this study are: i) What is the efficacy of kC-V and kC-AC hydrogels as filters for PFOA removal from aqueous solutions? ii) What is the influence of vanillin and AC concentration on kC hydrogel performance, and iii) What is the capability of kC hydrogels to treat PFOA-contaminated wastewater from soil remediation? The outcomes of this study will provide data about the feasibility of applying a kC-based gravity hydrogel filter as a potential technology for PFOA treatment. Furthermore, kC is environmentally friendly, cost-effective, and biodegradable, making it a sustainable water purifying option.

2. Material and methods

2.1. Materials

All materials in this research were procured from Sigma Aldrich Australia. The sulphated plant polysaccharide (kC), vanillin, and AC were acquired from the Australian branch of Sigma-Aldrich and utilized

in all experimental methods. The perfluorooctanoic solution (POFA) was prepared with different concentrations of 0.5, 1, and 1.5 mg/L to test it with the novel membrane filter to find the efficiency of rejection and flux. Polyvinyl alcohol solution (PVA) was obtained from Sigma Aldrich, Australia.

2.2. Hydrogel Fabrication

The kC hydrogel was prepared by dissolving 3 g in 100 mL (3% wt/v) of kC powder in deionized (DI) water. The dissolution process took place at temperatures between 60 and 80 °C. The mixture was then continuously stirred on a magnetic stirrer for 3 h at 800 rpm, forming a homogeneous hydrogelatinous solution (Fig. 1). It is worth noting that the hydrogelling temperature for kC typically falls within the range of 60–80 °C. Observations revealed that utilizing a higher temperature of 80 °C significantly impacted the separation performance of the hydrogel, which led to the formation of a more rigid hydrogel structure, the result of quick blockage of the filtration system.

In contrast, hydrogels synthesized at a lower temperature of 60 °C exhibited improved separation performance due to their comparatively softer and more flexible nature. The hydrogel was then subjected to purification steps, such as washing with DI water, to remove residual impurities. Finally, the hydrogel was characterized using various techniques, such as rheological analysis, microscopy, and spectroscopy, to evaluate it.

In a controlled experiment, 1%, 2%, and 3% vanillin and 0.1%, 0.2%, and 0.3% AC powder (weight/volume) were individually dissolved in deionized water (Fig. 1). The solutions were then incorporated into separate hydrogel matrices through vigorous mixing using a shaker apparatus. When kC was combined with either vanillin or AC, the respective molecules became entrapped within the three-dimensional structure of kC, forming distinct complexes. This complexation process led to notable alterations in the physical properties of kC, encompassing changes in viscosity and mechanical strength. Moreover, vanillin and AC exhibited specific interactions with kC chains, including hydrogen bonding, electrostatic attractions, and hydrophobic interactions. In the case of vanillin, hydrogen bonds formed between the sulphate groups of kC and the hydroxyl groups of vanillin, while AC showed adsorption onto the surface of kC. These interactions played pivotal roles in influencing the overall structure and properties of the respective composite materials. The kC-V and kC- AC hydrogel were carefully layered onto fabric support within a plexiglass column filtration setup 30 cm in

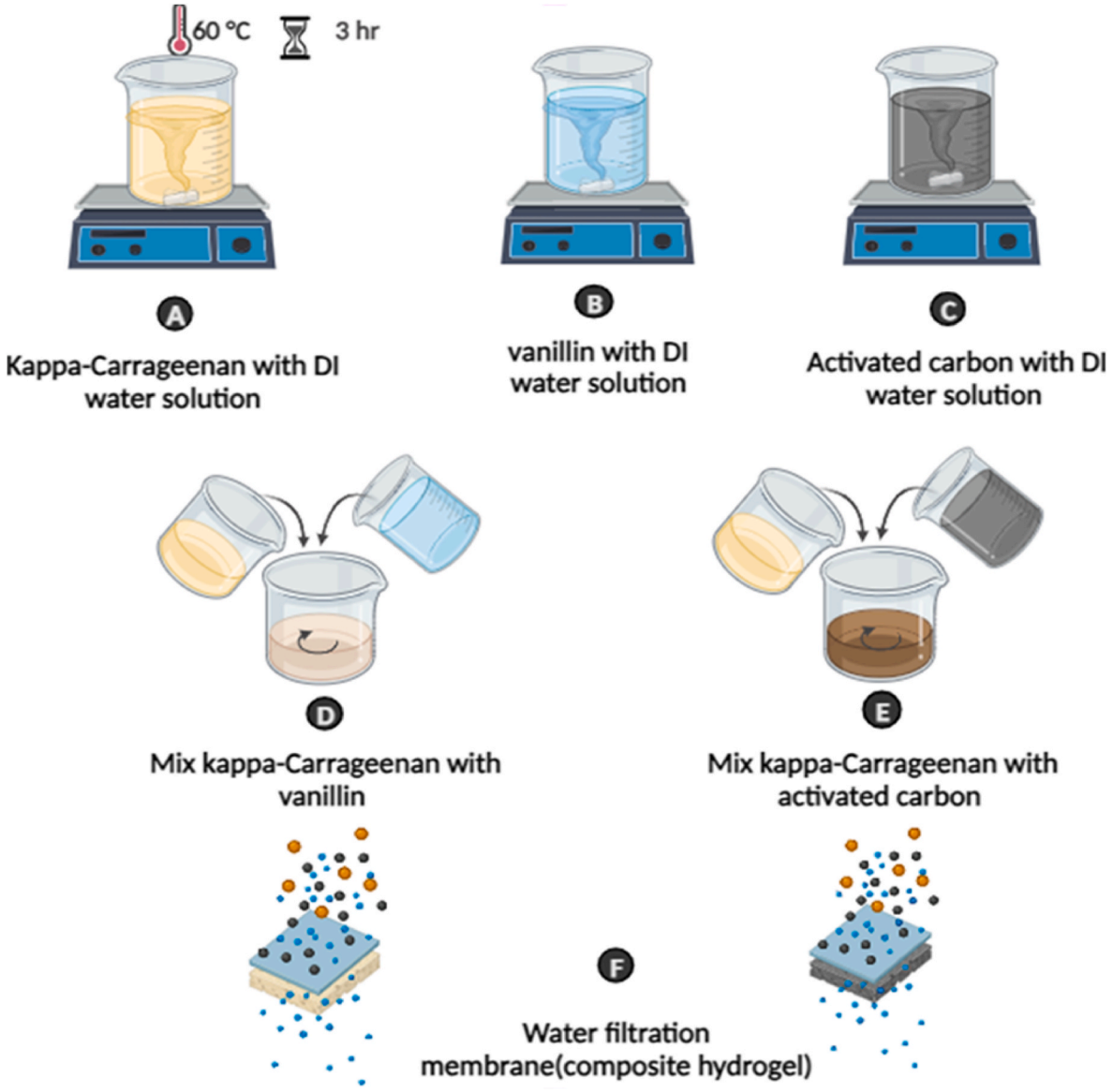

Fig. 1. Hydrogel fabrication.

height. With a filtration area of 0.0007 m^2, the hydrogel was given 10–15 min to settle and hydrate. Observational data revealed that water seepage through the column walls was occurring, potentially diminishing the efficacy of the filtration process. To address this issue, a PVA solution was applied to the outer edges of the hydrogel. Subsequently, pure water was introduced slowly to prevent any disruption to the hydrogel structure, ensuring optimal performance Fig. S1.

2.3. PFOA analysis

PFOA in water samples was analyzed by a triple quadrupole ultra-high-performance liquid chromatograph-tandem mass spectrometer (UHPLC-MS/MS) from Shimadzu (model 8060), following a method by Xu et al. (2020)(Xu et al., 2020). Compound separation was through a Shim-pack column (1.6 μm, 2.0 mm × 50 mm), using mobile phase A (Milli-Q water) and mobile phase B (methanol). Under a flow rate of 0.4 mL min^{-1}, samples of 1 μL were injected. The elution of PFOA from samples began with 50% B for 2.5 min, then 100% B for the next 1 min, followed by 50% B for another 1.5 min, with a total run time of 5 min. The mass spectrometer was operated in multiple reaction monitoring mode, using ions (*m/z* 169.1, *m/z* 219.0) as the qualitative ions and ion (*m/z* 369.0) as the quantitation ion. Quality assistance procedures included the regular checks of blanks, regular calibration by PFOA standards, and derivation of the limit of detection.

3. Methods of analysis for membrane characterization

3.1. Membrane morphology

The functional groups in kC gel, kC-V, and kC-AC were analyzed using FT-IR (Fourier Transform Infrared) with a Thermo Scientific Nicolet spectrometer. The spectrometer was equipped with an IR microscope with an optical resolution of 0.9 cm^{-1}. Before analysis, the samples were dried at 105 °C for 24 h. The study encompassed the wavenumber range of 4000-500 cm^{-1}. The gel samples were subjected to field-emission scanning electron microscopy (FE-SEM) using a Zeiss EVO LS15 SEM. Before imaging, a thin coating of gold with a thickness of 6 nm was applied to the samples using a sputtering machine. Three SEM tests were performed and averaged to generate the final spectra for precise outcomes. In addition, energy-dispersive X-ray spectroscopy (EDX) was performed on the same SEM samples using a Bruker SDD X flash 5030 detector. The TECHPoro Capillary Flow Porometer was utilized for pore size analysis, employing the BJH model for both the adsorption and desorption processes. The contact angles of 3%kC and kC with 1%–3% concentrations of vanillin and 0.1%–0.3% AC were measured to assess hydrogel surface wettability and hydrophilicity. The DM 211 contact angle measurement system (Kyowa Interface Science, Chennai, India) was used to measure water contact angles using the sessile-drop method. For each sample, a minimum of three locations were chosen to obtain contact angle measurements. The result was the average water contact angle with an error value.

3.2. Membrane porosity and pore size

The porosity of the hydrogel membrane was calculated by cutting the membrane into dimensional pieces of (3 × 3 × 1) cm and immersing it in distilled water for 15 h, then weighing it after removing all excess water on a surface using blotting paper (*weight1*). After that, it was dried in an oven at 60 °C for 6 h and weighed (*weight2*). The porosity was calculated by Equation (1).

$$P\% = \left(\frac{weight1 - weight2}{A^{*}l^{*}\rho}\right) \quad (1)$$

weight1 and *weight2* are the gel membrane's wet and dry weight values, respectively. *A* is the gel membrane sample area cm^2. *l* is the membrane thickness cm, and ρ is the water density (1 g/cm^3).

The gel membrane's average pore radius size rm was calculated using the membrane porosity and pure water flux through the membrane by Equation (2).

$$rm = \sqrt{\frac{(2.9 - 1.75p) \times (8 \times lQ\eta)}{(p \times A \times \Delta P)}} \quad (2)$$

ΔP is the operation pressure, p is the membrane porosity, and l and A are the membrane thickness and effective membrane area. Q is the volume of pure water flux per time (m^3/s)(Alsalhy et al., 2013).

3.3. Water uptake and swelling

Water uptake (WU) was determined using a previously dried membrane by cutting the membrane into dimensional pieces of (3 × 3 × 1) cm. The hydrogel pieces were dried in an oven at 105 °C for 6 h. Dry weight was recorded (*Wdry*). After drying, the pieces were immersed in distilled water for 24 h at room temperature and weighed after removing all excess water on a surface using blotting paper (*Wwet*). Finally, water uptake was determined using Equation (3). Three samples underwent testing, and the average outcomes were subsequently reported.

$$Wu = \left(\frac{Wwet - Wdry}{Wdry}\right) x100 \quad (3)$$

The hydrogel's swelling degree was also determined to assess its anti-swelling properties. The initial weight of the hydrogel (Winitial) was recorded, then placed in DI water and PFOA solution at 0.5, 1, and 1.5 mg/L concentrations for 2–24 h. The final weight (*Wfinal*) was re-recorded, and the swelling degree (*SD*) was estimated using Equation (4).

$$SD = \frac{(Wfinal - Winitial)}{Winitial} * 100 \quad (4)$$

3.4. Membrane performance efficiency

The kC-AC and kC-V hydrogel were cast on a fabric material with a pore size of about 30 μm, providing a support layer. Experimental work was conducted using a 30 cm tall homemade plexiglass column Fig. S1 with a filtration area of 0.0007 m^2 and a constant head of 30 cm, facilitating visual observation. The fabric support layer was tightly placed at the bottom of the column, and the kC-AC and kC-V hydrogel were poured slowly on top of the substrate. It was allowed to settle for 10–15 min while remaining hydrated. Care was taken to avoid sudden impacts that could deform the hydrogel and compromise its performance. Then, 1 mg/L PFOA solution was gradually poured onto the column for filtration. Analytical equipment measured the contaminants' water flux and rejection rate. All experiments were repeated at least three times to ensure reliability. The water flux was determined using the provided Equation (5).

$$J = \frac{V}{A^{*}t} \quad (5)$$

V represents the accumulated permeate volume (m^3) over time (t), and A denotes the efficient membrane area (m^2) utilized in the filtration process. The rejection of pollutants was measured using Equation (6).

$$R\% = \left(1 - \frac{Cp}{Cf}\right) * 100 \quad (6)$$

In Equation (6), *Cp* refers to the pollutant concentration in the permeate solution, and Cf is the initial concentration of the same contaminants in the feed solution. Experiments were repeated at least three times for water flux rejection studies.

3.5. PFOA-contaminated water

The perfluorooctanoic acid (PFOA) solution was prepared at concentrations of 0.5, 1, and 1.5 mg/L to evaluate the novel membrane filter's efficiency in terms of rejection and flux. PFOA quantification was performed using liquid chromatography-mass spectrometry (LC-MS). Calibration curves for PFOA quantification were established using a six-point calibration range from 5 μg/L to 50 μg/L. The data were fitted to a quadratic, weighted regression equation. The calibration curve's coefficient of determination (R^2) exceeded 0.99 in all analyses. The accuracy for PFOA analysis across all quality control (QC) concentration levels was within ±5%.

The hydrogel membrane was tested with PFOA-contaminated wastewater from electrokinetic soil remediation in Sydney, Australia. Liquid chromatography-mass spectrometry (LC-MS) and inductively coupled mass spectroscopy (ICP-MS) were used to measure the PFOA and metal concentrations, respectively (Table 1).

4. Statistical assessment

Every experiment was replicated at least three times, and the outcomes are presented as the mean values. The Analysis of Variance (ANOVA) was employed to assess variations among multiple experimental data sets. Single-factor ANOVA analysis for experimental data showed a *P-value* less than 0.05, indicating statistically significant differences between treatment groups.

5. Results and discussion

5.1. Hydrogel membranes characterization

FE-SEM analysis examined the surface morphology of the kC-AC and kC-V hydrogels after drying for 24 h at 60 °C, during which it experienced shrinkage. Fig. S2 (Supplementary Materials) shows the surface of the pure kC hydrogel, which exhibits a relatively smooth texture with irregular folds and indications of brittle fractures. The SEM image in Fig. 2a illustrates the presence of diminutive nanostructures composed of vanillin in the uppermost layer of the hydrogel surface and configurations like canals and valleys to facilitate the entrapment of contaminants. This structural arrangement resembles a thin-film composite membrane characterized by ridge and valley-like topography (Hamid et al., 2021). Fig. 2c describes the surface of kC-0.3%AC hydrogel, which has diverse properties, including roughness and porosity. AC becomes an integral part of the kC matrix, featuring irregularly shaped particles with porous structures, while kC particles exhibit organized, helical structures. Notably, SEM images unveil the existence of pores or voids within the composite, impacting its adsorption capacity, particularly when AC assumes the role of the adsorbent. Fig. 2b and d shows the alteration of kC-AC and kC-V hydrogel surface morphology after PFOA filtration, including swelling, pore size, and surface roughness. It provides evidence of PFOA adsorption on the hydrogel's surface, manifested by potential pore blockage.

Table 1
PFOA-contaminated water analysis and composition.

Parameter	Measurement tool	Value
pH	LAQUA-pH meter (Horriba, Japan)	9.53
Conductivity	LAQUA meter (Horriba, Japan)	1.871 ± 2 ms/cm
Total dissolved Solids	LAQUA meter (Horriba, Japan)	1774 ± 5 mg/L
Turbidity	Turbidity meter (Horriba, Japan)	>100 ± 2 NTU
PFOA	LC-MS	179.2 ± 3 mg/L
Na	ICP-MS (Agilent, United States)	25 ± 5 mg/L
K	ICP-MS (Agilent, United States)	18 ± 5 mg/L
Si	ICP-MS (Agilent, United States)	10 ± 5 mg/L
Cl	ICP-MS (Agilent, United States)	33 ± 5 mg/L
Al	ICP-MS (Agilent, United States)	104 ± 5 mg/L

The Fourier-transform infrared spectroscopy (FT-IR) analysis of the kC-(1–3)%V hydrogel confirmed the presence of discernible peaks (Fig. 2e). The heightened peaks indicated the interaction between vanillin and kC, particularly increased hydroxyl groups' intensity at 3200–3600 cm^{-1}. This analysis aligns with the theory of hydrogen bonding, suggesting that vanillin contributes to the hydroxyl groups. Furthermore, vanillin acted as a pore-forming agent, enhancing hydrogel hydrophilicity and biocidal properties. Studies showed increased membrane porosity due to vanillin concentration, attributed to the polar functional groups like alcohols and aldehydes, resulting in a negatively charged membrane surface (Zhang et al., 2022). Compared to kC spectra, new peaks were observed in kC-1%V, while kC-2%V and kC-3%V exhibited similar profiles. A broad peak at 3765 cm^{-1}, representing hydroxyl (OH) groups, was slightly increased in the presence of vanillin.

FT-IR analysis of the kC-(0.1–0.3)%AC hydrogel offers valuable molecular insights. The kC exhibits - OH groups as a broad absorption band 3000–3500 cm^{-1} signifying O–H stretching vibrations. The spectrum reveals strong absorption of 1240–1260 cm^{-1} corresponding to sulphate ester bonds (O═S═O) in kC, referring to potential interactions with AC. In the 1600–1800 cm^{-1} range, absorption bands arise from carbonyl (C═O) stretching vibrations originating from various kC and AC surface functional groups (e.g., COOH, OH, C═O). AC introduces distinctive peaks, representing its surface functional groups, notably COOH, OH, and C═O (Fig. 2f). Tracking any shifts or changes in absorption bands during FT-IR analysis can reveal chemical interactions between kC and AC, including hydrogen bonding or chemical adsorption. Zhou's study highlighted the complexity of AC adsorption, driven by diverse forces. The AC surface primarily features oxygen-containing functional groups such as carbonyl, carboxyl, lactone, and phenolic hydroxyl, influencing its adsorption capabilities (Zhou et al., 2021).

5.2. Contact angle and rheology

The hydrogel's surface hydrophobicity was determined by measuring the water contact angle (Fig. 3a and b). According to Bhushan et al. (2011), a contact angle between 0° and 90° indicates a hydrophilic surface, while angles exceeding 90° indicate hydrophobicity. Surface wettability is influenced by chemical composition and morphology, with roughness affecting contact angles through models like the Wenzel or Cassie–Baxter models (Bhushan and Yong Chae, 2011). kC's chemical structure imparts hygroscopic properties, making hydrogel surfaces wets hydrophilic with a measured contact angle of 72°. AC has both hydrophobic and hydrophilic sites on its surface. While it naturally leans towards hydrophobicity, filtration processes demand hydrophilic characteristics for enhanced performance, achievable through various treatments (Kostov et al., 2014). Incorporating 0.1–0.3% of AC into a kC solution decreased the contact angle to 53.8° ± 3 for 0.1%AC, followed by a slight increase to 55.5° ± 3 for 0.2%AC and 57.4° ± 3 for 0.3%AC. Adding 1%–3% vanillin to kC hydrogels substantially reduced the water contact angle (Fig. 3a and b), mainly due to vanillin's high hydrophilicity. The results align with previous studies that showed reduced contact angles when vanillin was added to Polysulfone (PSf) membranes (Yadav et al., 2022). The most significant decrease in hydrophobicity was observed in the kC-1%V hydrogel, resulting in a water contact angle of 58° ± 3. Increasing vanillin concentrations in the hydrogel led to a slight decrease in contact angles for the kC-2%V and kC-3%V hydrogels, reaching 55° ± 3 and 53° ± 3, respectively. During phase inversion, vanillin's hydrophilic nature migrated to the surface, enhancing membrane hydrophilicity (Arthanareeswaran et al., 2009).

Essential to understanding the rheological properties of the kC response to shear forces and deformation when combined with vanillin or AC, examining changes in its viscosity that measures resistance to flow and shear stress that characterizes the internal stress when subjected to mechanical forces. Adding vanillin to the kC hydrogel increased viscosity and was further amplified upon adding AC (Fig. 3c and d). The viscosity for all hydrogel decreased with increased shear

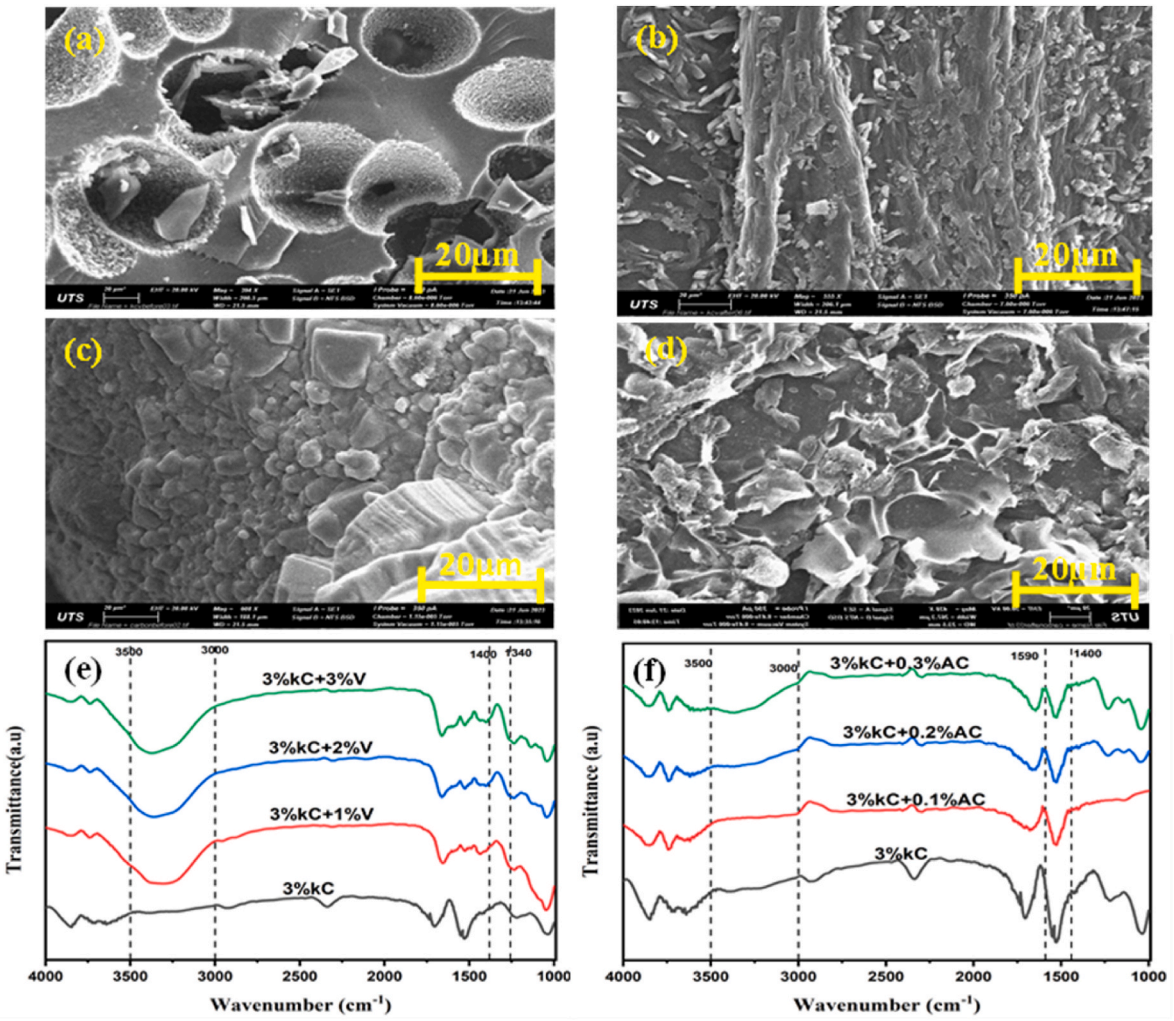

Fig. 2. SEM and FT-IR analysis of the hydrogel, a) SEM of the kC-3% V hydrogel before filtration at 20 µm at the first focus point, b) SEM of the kC-3% V hydrogel after filtration at 20 µm at the first focus point, c) SEM of the 3%kC-0.3%AC hydrogel before filtration at 20 µm at the first focus point, d) SEM of the 3%kC-0.3%AC hydrogel after filtration at 20 µm at the first focus point, e) FT-IR of kC-(1–3)%V before filtration, f) FT-IR of kC-(0.1–0.3)%AC before filtration.

stress; for the middle point in the graph, the viscosity values of kC, kC-3%V, and kC-0.3%AC were 61116 mPa s, 187430 mPa s, and 420610 mPa s, respectively. The corresponding shear stress for the 3%kC, kC-3% V, and kC-0.3%AC hydrogels was 136.4 Pa, 419.63 Pa, and 941.46 Pa, respectively, closely related to water contact angle changes. Notably, the viscosity properties exhibited marked distinctions compared to the hydrogel without vanillin or AC serving as controls.

5.3. Porosity and pore size

Fig. 3e and f depict vanillin and AC influence on the porosity of kC membranes. The introduction of 1%–3% vanillin into the kC hydrogel enhanced the membrane porosity from 62.8% ± 5–75.8% ± 5, 77.5% ± 5, and 79.1% ± 5. Similarly, the incorporation of 0.1%–0.3% AC into the kC hydrogel increased the porosity from 62.8% ± 5–85.4% ± 5, 87.6% ± 5, and 89.7% ± 5, respectively. Hydrophilic additives help expedite solvent-nonsolvent exchange in hydrogels and facilitate the formation of highly porous membrane structures.

Furthermore, the increase in porosity is accompanied by a gradual transition in void morphology within the membranes, shifting from microcavities to valley-like voids characterized by a more constrained size distribution. According to Equation (2) and Fig. 3e and f, the pore radius for kC was 3.2 nm ± 1, kC-(1–3)%V was 2.63 nm ± 1, 2.59 nm ± 1, 2.57 nm ± 1, and kC-(0.1–0.3)%AC was 1.95 nm ± 1, 1.86 nm ± 1, 1.68 nm ± 1, respectively. Membranes featuring a confluence of smaller, uniformly dispersed pores tend to exhibit elevated porosity due to the abundance of void space within the matrix. Conversely, membranes characterized by larger or irregularly distributed pores often yield lower porosity. This matches the results obtained for both hydrogels composite. Surface area is a crucial parameter that characterizes the surface properties of an adsorbent. The Brunauer-Emmett-Teller (BET) method is widely employed for quantifying the surface area of an adsorbent, utilizing nitrogen gas as an adsorbate interacting with the material's surface. The specific surface area of kC is 10.872 m^2/g, 33.15 m^2/g for kC-3%V, and 95.61 m^2/g for kC-0.3%AC (Table 2). In addition, the total pore volume of the kC hydrogel is 0.015 cc/g compared to 0.047 cc/g and 0.099 cc/g for the kC-3%V and kC-0.3%AC.

5.4. Water uptake and swelling degree

Water uptake for the kC hydrogel composite represents its ability to absorb and retain water, a critical attribute determined by factors such as hydrogel concentration, formulation, and environmental conditions. The kC-AC and kC-V composite hydrogels of equal thickness of 2 cm were tested for the water uptake capacity. The hydrogel contracted during drying, folding at the edges and transforming into a compact, plastic-like structure (Fig. 4a and b). The impact of different concentrations on swelling degree is reported in Fig. 4c and d; water uptake

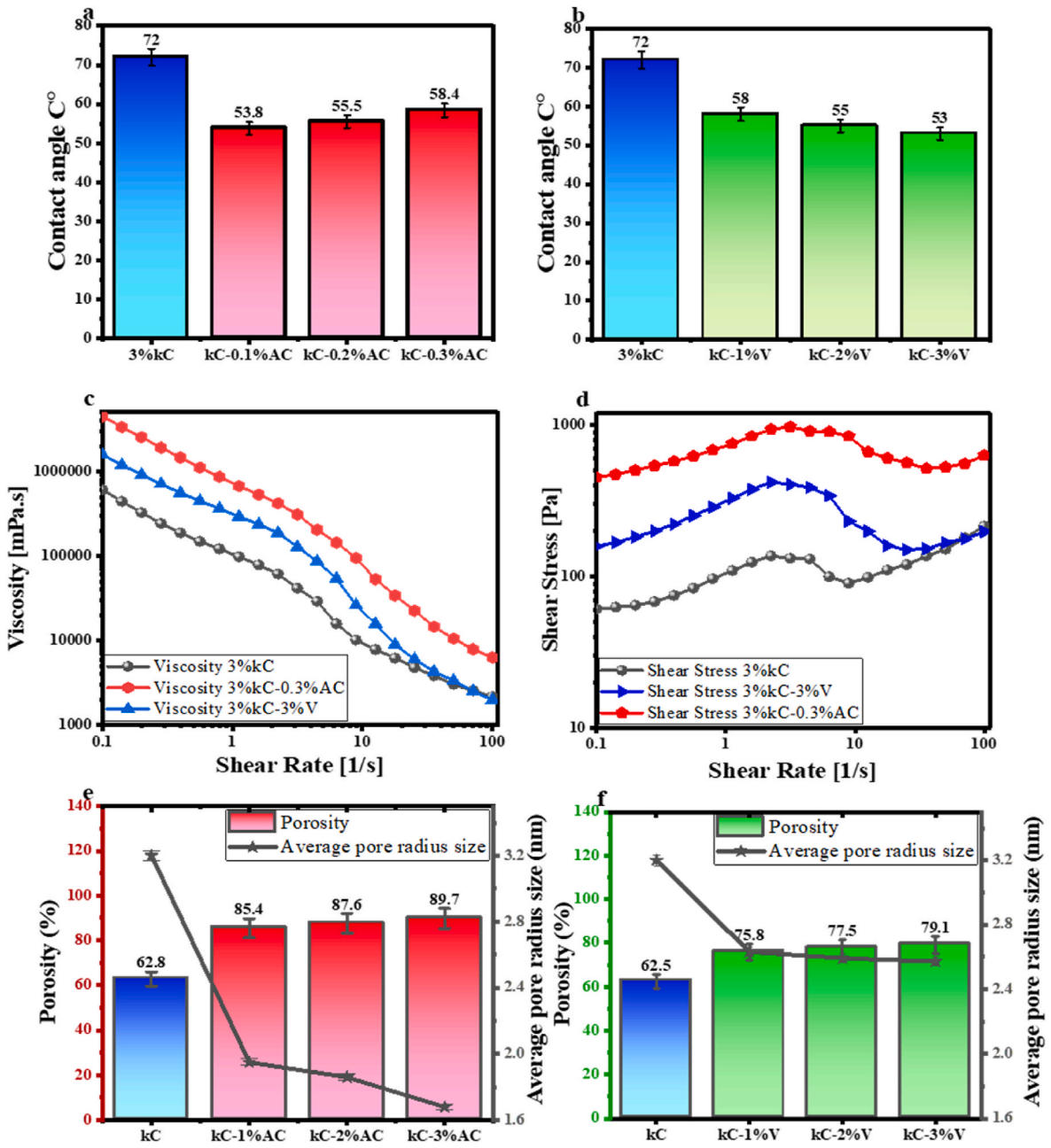

Fig. 3. a) the contact angle for the 3% kC, 3% kC-AC, b) the contact angle for the 3%kC-V, c,d) viscosity and shear stress of the composite hydrogel, e) the effects of AC content on the porosity and average pore size of kC-AC membranes, f) the effects of vanillin content on the porosity average pore size of kC-V membranes. The error bar = 1 standard deviation.

Table 2
Adsorption and Desorption summaries of BET analysis.

BET analysis		3%kC	3%kC-3%V	3%kC-0.3%AC
Adsorption summary BJH	Surface area	10.872 m^2/g	33.15 m^2/g	95.61 m^2/g
	Pore Volume	0.015 cc/g	0.047 cc/g	0.099 cc/g
	Pore Diameter	3.231 nm	3.228 nm	5.83 nm
Desorption summary BJH	Surface area	5.776 m^2/g	23.7 m^2/g	60.80 m^2/g
	Pore Volume	0.009 cc/g	0.036 cc/g	0.0504 cc/g
	Pore Diameter	3.309 nm	3.318 nm	3.492 nm

increases with the increasing vanillin and AC concentrations. The kC-(1–3)%V hydrogel exhibited 966.22% ± 2, 1038.8% ± 2, and 1045.5% ± 2, water uptake, respectively. The corresponding kC-(0.1–0.3)%AC results were 892.31% ± 2, 902.2% ± 2, and 918.4% ± 2, respectively. The kC-3%V and kC-0.3%AC displayed an exceptional water uptake capacity, absorbing 1045.5% ± 2 and 918.4% ± 2 of water, significantly outperforming most hydrogels. This increase in water uptake implies an enhanced proton diffusion rate facilitated by hydrogen bonding with water molecules and increased hydroxyl ion flux, causing distinct water-absorbing capabilities for different formulations of the kC hydrogel. Hydroxyl groups in the hydrogel enhance its hydrophilicity, increasing water uptake as the nanoparticle percentage rises. Vanillin and AC, forming hydrogen bonds with kC, boost water uptake in the composite hydrogel. Higher vanillin and AC concentrations significantly amplify water uptake. The relationship between water uptake and sulphate

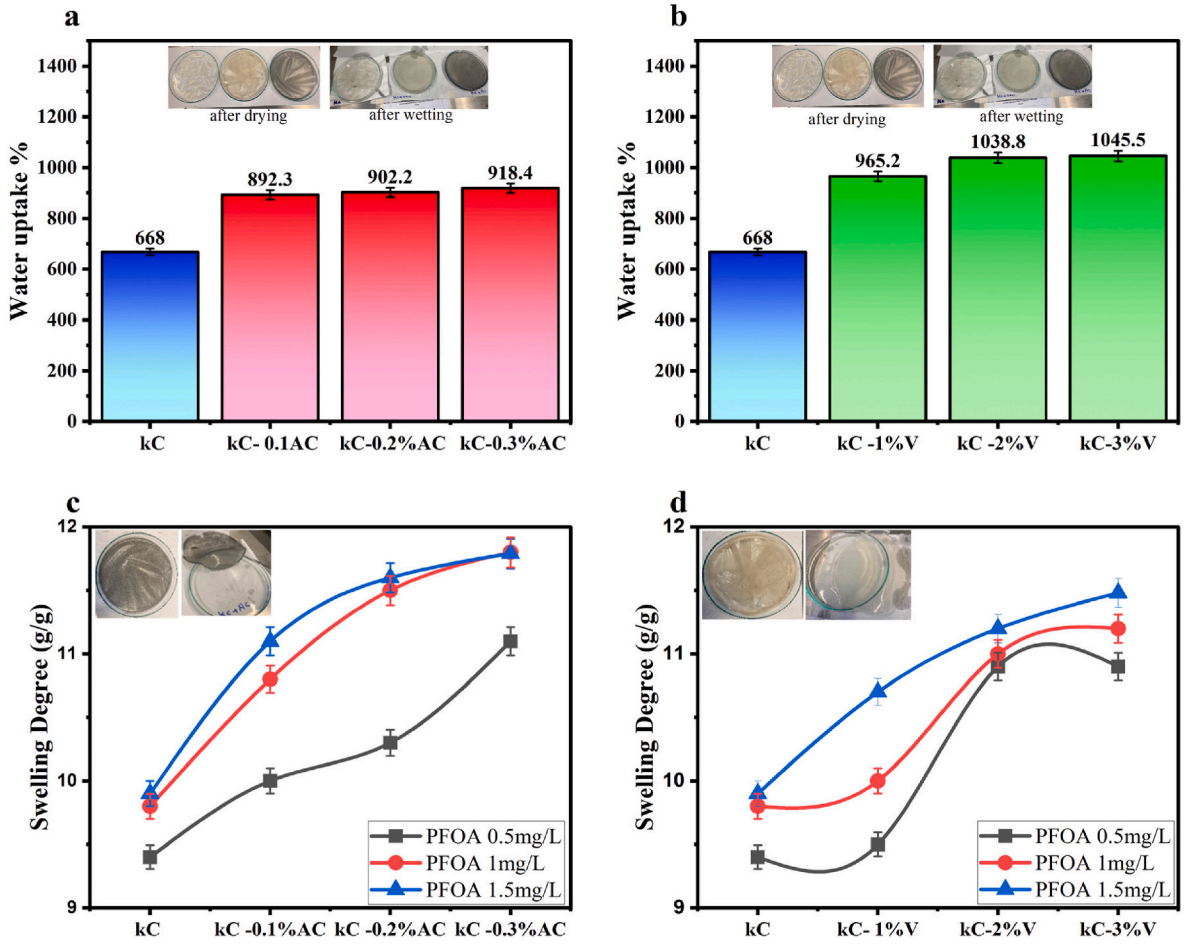

Fig. 4. a) Water uptake of different concentrations of kC-AC hydrogel, b) Water uptake of different concentrations of kC-V hydrogel, c) Swelling degree of kC with various concentrations of AC at different concentrations of PFOA, d) Swelling degree of kC with various concentrations of vanillin at different concentrations of PFOA. The error bar = 1 standard deviation.

group content varies, as sulphate content affects moisture absorption differently. The sulphate content, molecular weight, crosslinking percentage, and microstructure void volume influence moisture content in polysaccharide hydrogels. The hydrogel's structure and chemical composition are vital in water uptake properties (Balasubramanian et al., 2018).

The swelling degree measures how much a hydrogel expands when exposed to a solvent, typically expressed as the ratio of the swollen volume to its initial dry volume. Factors like polymer network structure, ionic groups, and solubility influence this degree. In loosely crosslinked domains, polymer chains deform more upon swelling than densely crosslinked domains. The kC-based hydrogels consist of polymer chains with charged sulphate groups that repel each other due to their negative charge. The electrostatic repulsion increases the distance between chains, making the network more permeable to large molecules and allowing more water to enter, resulting in a higher swelling degree. The maximum swelling degree was observed to rise with longer sub-chain lengths, representing the length of chains between crosslinks. The introduction of PFOA into a hydrogel may also impact its swelling degree. PFOA's hydrophobic properties can diminish the hydrogel's attraction to water, potentially reducing swelling. However, it's essential to consider that the concentration of PFOA and the specific polymer chemistry of the hydrogel will determine the extent of this effect. Swelling studies have shown that hydrogel composites achieve equilibrium swelling after being immersed overnight in different PFOA concentrations (0.5, 1, 1.5) mg/L. Fig. 4c and d illustrate the extent of swelling in kC-AC and kC-V hydrogel composites. Among the kC-AC formulations, the kC-0.3% AC hydrogel demonstrated the highest swelling degree of 11.8 ± 1 g/g when exposed to 1 mg/L of PFOA. This result was statistically significant when compared to other kC-AC formulations.

Additionally, hydrogels exposed to PFOA concentrations of 0.5 and 1.5 mg/L exhibited 11.1 ± 1 g/g and 11.8 ± 1 g/g swelling, respectively, with minimal variations in sol fraction over time. The swelling of the kC-V hydrogels was assessed by immersing them in a PFOA solution for 24 h (Fig. 5d). The kC-3%V hydrogel displayed favourable swelling behaviour of 11.5 ± 1 g/g, outperforming the kC-2%V and the swelling of the kC-1%V hydrogel of 11.2 ± 1 g/g and 10.7 ± 1 g/g, respectively. This behavior is attributed to hydrophilic functional groups, including –OH, $–CONH_2$, $-CONH^-$, and $-SO^3$ (Hamidi et al., 2008).

5.5. kC-AC and kC-V performance

Several factors, including hydrogel thickness, feed concentration, pH of the feed solution, solute volume, viscosity, and ionic interactions, influence the water flux of the hydrogel. In the filtration experiments, the hydrogel membrane was tested with PFOA-contaminated wastewater from soil remediation. A support layer made of fabric material with a pore size of 30 μm was selected for the kC-V and kC-AC hydrogel membrane filter. The hydrogel was manually applied to the fabric layer within a specialized filtration column designed for water treatment. This support layer serves as a structural foundation for the hydrogel during filtration.

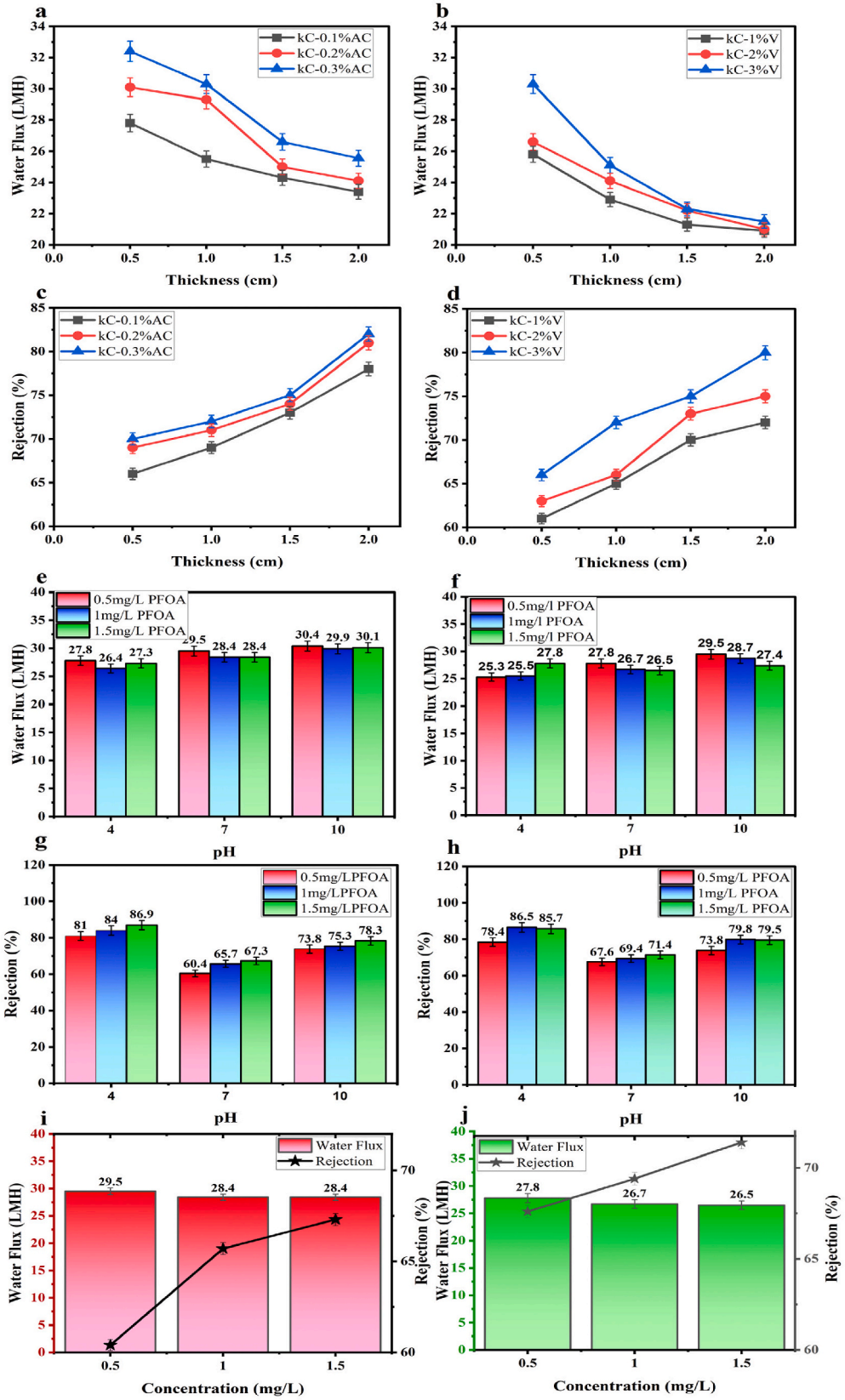

Fig. 5. a) The impact of kC-AC hydrogel thickness on water flux with a 1 mg/L PFOA, b) The impact of kC-V hydrogel thickness on water flux with a 1 mg/L PFOA, c) The impact of kC-AC hydrogel thickness on 1 mg/L PFOA rejection, d) The impact of hydrogel thickness (kC-V) on 1 mg/L PFOA rejection, e) The influence pH of a PFOA feed solution on water flux for kC-0.3%AC hydrogel, f) The influence pH of a PFOA feed solution on water flux for kC-3%V hydrogel, g) The influence pH of a PFOA feed solution on rejection for kC-0.3%AC hydrogel, h) The influence pH of a PFOA feed solution on rejection for kC-3%V hydrogel, i) Effect (0.5, 1, 1.5) mg/L PFOA concentration on water flux rate and rejection of 2 cm thick kC-0.3%AC hydrogel, j) Effect (0.5, 1, 1.5) mg/L PFOA concentration on water flux rate and rejection of 2 cm thick kC-3%V hydrogel. The error bar = 1 standard deviation.

5.5.1. Effect of hydrogel thickness

A feed solution containing 1 mg/L of PFOA was employed to evaluate water flux at 0.5 cm, 1 cm, 1.5 cm, and 2 cm hydrogel thicknesses. The height of the filtration column was 30 cm (0.029 bar. The hydrogel comprises a 3% kC, blended with 1%–3 % vanillin or 0.1%–0.3% AC. Hydrogel thicknesses were examined to determine the optimal water flux and rejection performance. There is a trade-off between the hydrogel water flux and rejection as the membrane thickness increases from 0.5 cm to 2 cm (Fig. 5a and b). In general, the results demonstrate that a substantial enhancement in the water flux can be achieved by increasing the vanillin and AC content within the kC hydrogel. For example, the water flux in the kC-0.3%AC decreased from 32.4 LMH in 0.5 cm hydrogel thickness to 25.6 LMH in 2 cm kC-0.3%AC thickness (Fig. 5a). On the contrary, water flux increased with increased AC and vanillin concentration in the kC hydrogel. The water flux was 23.4 LMH in the kC-0.1%AC, 24.1 LMH in the 0.2%AC, and 25.6 LMH in the kC-0.3%AC (Fig. 5a). The corresponding water flux for kC-V hydrogel was 20.9 LMH for kC-1%V, 21 LMH for kC-2%V, and 21.5 LMH for kC-3%V.

Increasing the water flux with the AC and vanillin concentration in the hydrogel is attributed to increased surface hydrophilicity, pore density, porosity, and macro voids, alongside the formation of vertically interconnected finger-like pores (Zhu et al., 2021). Due to enhanced membrane hydrophilicity, the water flux in the kC-3%V and kC-0.3%AC membranes achieved 25.6 LMH ±2 and 21.5 LMH ±2, respectively. These outcomes align with the increase in porosity and pore size radius for hydrogels composite, which were 89.7% and 1.68 nm in kC-0.3%AC, 79.1% and 2.57 nm in kC-3%V, 1.68 nm. The water flux enhancement is facilitated by vanillin and AC additives that accelerate solvent exchange during membrane preparation, increasing porosity and larger cavities. Also, the structural changes in the membrane's cross-morphology, from delicate finger-shaped pores in the kC membrane to broader valley-shaped pores with macro voids in kC-AC and kC-V membranes, facilitate smoother water molecule passage, further increasing water flux, and Fig. 2a and c confirm that. Although water flux increased the AC and vanillin concentration in the hydrogel, PFOA adsorption reduced water flux due to pore narrowing, exacerbated by higher AC or vanillin particle concentrations, resulting in a rougher membrane texture. Besides, adding vanillin plays a pivotal role in the generation of pores and the augmentation of permeation rate (R et al., 2017). Adding vanillin imparts a negative charge to the hydrogel surface, increasing the hydrophilicity of hydrogel (Yadav et al., 2022). The interaction between kC and vanillin further enhances membrane permeability and fortifies its resistance to fouling (Alam et al., 2017; Yadav et al., 2022). When combined with kC, AC provides a robust framework for the entrapment of impurities due to its vast surface area and high porosity. The porous architecture of kC and AC improves the hydrogel's permeability, allowing water to pass while retaining contaminants (Mahdavinia et al., 2015).

The results demonstrate that a substantial enhancement in rejection was achieved by increasing the hydrogel thickness or the concentration of AC and vanillin due to the increased hydrogel adsorption capacity (Supplementary Materials S3.1). For example, the rejection in the kC-0.3%AC increased from 70% in 0.5 cm hydrogel thickness to 82% in 2 cm kC-0.3%AC thickness (Fig. 5c). On the contrary, rejection increased with increased AC and vanillin concentration in the kC hydrogel. The rejection was 78% in the kC-0.1%AC, 81% in the 0.2%AC, and 82% in the kC-0.3%AC (Fig. 5c). The corresponding rejection for kC-V hydrogel was 72% for kC-1%V, 75% for kC-2%V, and 80% for kC-3%V (Fig. 5d). The results showed that 2 cm hydrogels demonstrated superior PFOA rejection compared to thinner hydrogels, i.e., 0.5 cm, 1 cm, and 1.5 cm. A 2 cm thickness is optimal for achieving high water flux and rejection, as Fig. 5a,b,5c, and 5d illustrate. Although the contact angles of kC-AC and kC-V hydrogels were very close (Fig. 3a and b), the kC-AC exhibited greater water flux than kC-V due to the higher porosity (Fig. 3e and f). Also, kC-AC hydrogels exhibited more PFOA rejection than kC-V hydrogels because of i) the smaller average pore size of kC-AC hydrogels (Fig. 3e and f) and ii) the higher adsorption capacity of kC-AC hydrogel compared to kC-V (Fig. 6a and b). Therefore, kC-AC hydrogel exhibited better water flux and rejection rates than kC-V.

5.5.2. Effect of feed pH

A feed solution containing 0.5 mg/L, 1 mg/L, and 1.5 mg/L of PFOA was used in the 3%kC-0.3%AC and 3%kC-3 %V hydrogels to evaluate water flux and PFOA rejection at different feed pHs. Changing the feed pH can affect the electrostatic interactions between the membrane and PFOA compounds (Ouyang et al., 2019; Zhao et al., 2011). The pH was adjusted to pH 4, 7, and 10 to assess the hydrogel's performance using 0.1 M NaOH and 0.1 M HCl. The alkalinity of the feed solution can significantly impact the performance of the filtration process due to the change in surface charge, pore size, water flux, and rejection rates. For 2 cm hydrogel thickness, results show an increase in water flux with a pH increase and an increase in rejection with a pH decrease. The 2 cm hydrogel thickness results show increased water flux at alkaline pH and PFOA rejection at acidic pH (Fig. 5e, f, 5g, and 5h).

In general, the results demonstrate that a substantial enhancement in the water flux can be achieved at feed pH 10 and PFOA concentration 0.5 mg/L. For example, the water flux in the kC-0.3%AC increased from 27.8 LMH at feed pH 4 to 30.4 LMH at feed pH 10 (Fig. 5e). On the contrary, water flux decreased with increased PFOA concentration in the feed solution. The water flux at feed pH 10 was 30.4 LMH at 0.5 mg/L, 29.9 LMH at 1 mg/L, and 30.1 LMH at 1.5 mg/L PFOA (Fig. 5e). The corresponding water flux for kC-3%V hydrogel was 29.5 LMH at 0.5 mg/L, 28.7 LMH at 1 mg/L, and 27.4 LMH at 1.5 mg/L PFOA (Fig. 5f).

For kC-0.3%AC and kC-3%V hydrogels, results show PFOA rejection increased at pH 4 and decreased at pH 10 (Supplementary Materials S3.2). For example, the rejection in kC-0.3%AC at pH 4 was 86.9%, while it decreased to 78.3% at pH 10 for 1.5 mg/L PFOA concentration. In contrast, the rejection in kC-3%V hydrogel was 85.7% at pH 4 and decreased to 79.5% at pH 10. The results also exhibit a substantial rejection enhancement was achievable at increased PFOA concentration. For example, the kC-0.3%AC rejection of PFOA increased from 81% at 0.5 mg/L feed solution to 86.9% at 1.5 mg/L. Similarly, in the kC-3%V hydrogel, the rejection increased with increasing PFOA concentration. For example, the PFOA rejection was 78.4%, 86.5%, and 85.7% in 0.5 mg/L, 1 mg/L, and 1.5 mg/L, respectively (Fig. 5g and h).

The surface charge of a membrane, determined by functional groups and pKa, significantly influences PFOA separation efficiency based on the feed pH. Moreover, pH alterations impact membrane pore size, affecting PFOA removal. A positively charged surface enhances rejection through electrostatic attraction. Acidic feed pH also reduces the repulsion forces, causing pore shrinkage and improved rejection, while higher pH increases hydrogel porosity, resulting in a lower PFOA rejection. The pH-dependent behaviour of hydrogel ionizable groups influences the solvent flow and PFOA interactions, leading to varying rejection rates. Thus, pH is a crucial parameter in membrane and hydrogel filtration for effective PFAS removal (Jin et al., 2021; Pensini et al., 2019; Yang et al., 2017; Zeng et al., 2017a, 2017b).

5.5.3. Effect of feed concentration

To investigate the effects of the PFOA feed concentration on the water flux and rejection by KC-0.3%AC and kC-3%V hydrogels, 0.5, 1, and 1.5 mg/L PFOA concentrations were tested (Fig. 5i and j). For the kC-0.3%AC at 2 cm thickness and pH 7, The water flux slightly decreased with increasing the PFOA concentration, and it was 29.5 LMH ±0.5 at 0.5 mg/L, 28.4 LMH ±0.5 at 1 mg/L, and 28.4 LMH ±0.5 at 1.5 mg/L. On the contrary, PFOA rejection increased with an increase in the PFOA concentration, and it was 60.4 % ± 1 at 0.5 mg/L, 65.7 % ± 1 at 1 mg/L, and 67.3 % ± 1 at 1.5 mg/L. For KC-3%V at 2 cm and pH 7, the water was 27.8 LMH ±0.25 at 0.5 mg/L, 26.7 LMH ±0.25 at 1 mg/L, and 26.5 LMH ±0.25 at 1.5 mg/L. The corresponding PFOA rejection was 67.6% ± 0.25 at 0.5 mg/L, 69.4 % ± 0.25 at 1 mg/L, and 71.4 % ± 0.25 at 1.5 mg/L. Also, higher PFOA feed concentration decreases water

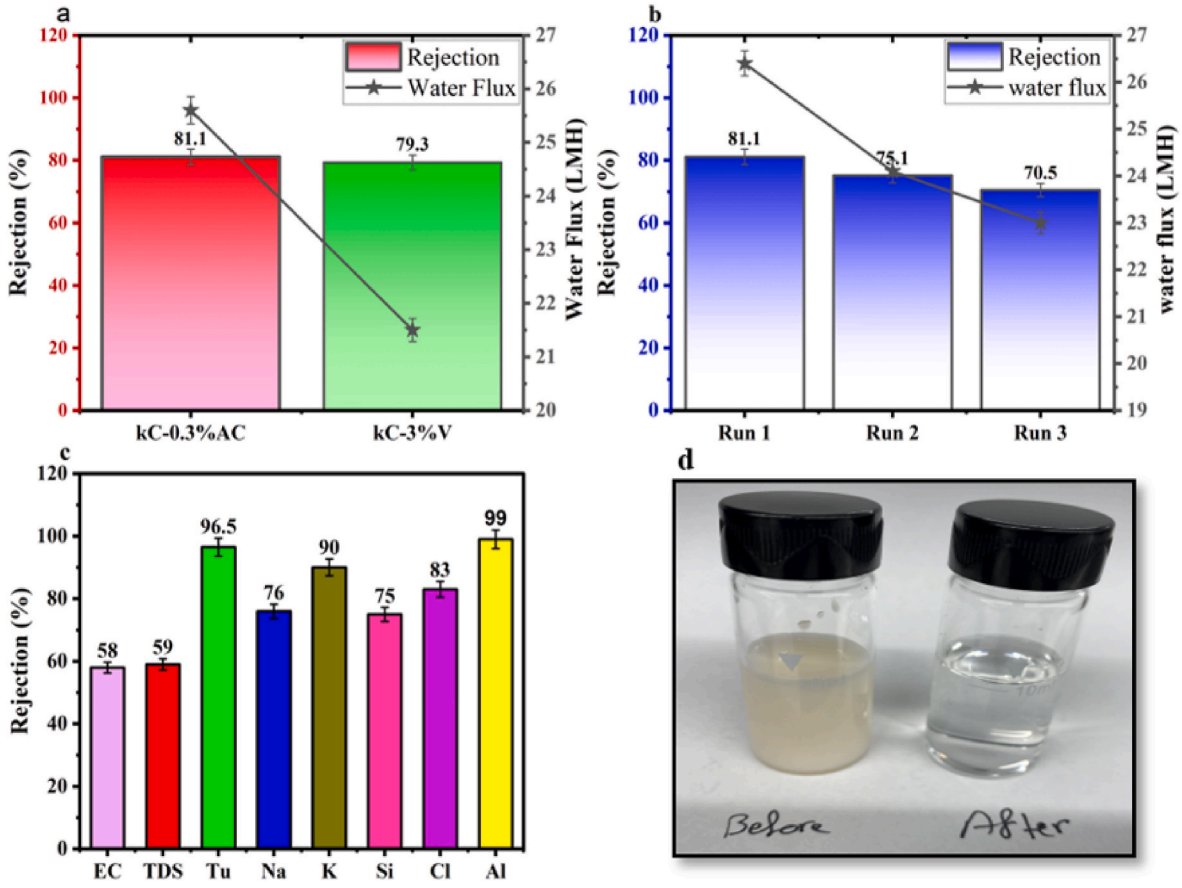

Fig. 6. a) Water flux rate and rejection of kC-0.3%AC and kC-3%V hydrogel for PFOA wastewater, b) Water flux and rejection in multiple cycles for PFOA feed solution in kC-0.3%AC, c) Rejection of elements and parameters from the PFOA-contaminated water kC-0.3%AC, and d) colour and turbidity rejection. The error bar = 1 standard deviation.

flux since it occupies available pore spaces, restricting the passage of water. Increased solute concentration reduces the effective hydrogel porosity. However, the reduction in porosity reduces permeability, i.e., water flows more slowly through the hydrogel, increasing the likelihood of interactions between the solutes and the hydrogel. These interactions can result in more significant adsorption or trapping of solutes within the hydrogel structure, leading to better removal efficiency. Therefore, the hydrogel's rejection capability increases with increasing the PFOA concentration. The results also agree with the literature (AlSawaftah et al., 2021; Eke et al., 2020) that delved into the PFAS removal efficiency in scenarios involving elevated 100 mg/L PFOA concentration. The potential for micelle formation arises at such PFOA concentrations, particularly as the concentration surpasses the critical micelle concentration threshold.

5.6. PFOA-contaminated water treatment

A 2 cm hydrogel gravity filter of 30 cm height was employed to remove 179.2 mg/L PFOA from electrokinetic soil-remediation wastewater. The kC-0.3%AC hydrogel exhibited excellent performance with 25.6 LMH ±1 water flux and 81.1% PFOA rejection (Fig. 6a). The corresponding water flux and rejection for kC-3%V hydrogel were 21.5 LMH±1 and 79.3%, respectively. The water flux enhancement in the kC-0.3%AC hydrogel is facilitated by AC, which accelerates solvent exchange during membrane preparation, increasing porosity and creating larger cavities (Table 2). Also, the structural changes in the membrane's cross-morphology, from delicate finger-shaped pores in the kC membrane to broader valley-shaped pores with macro voids in the kC-0.3% AC filter, facilitate smoother water molecule passage. Compared to kC-3%V hydrogel, kC-0.3%AC hydrogel showed better PFOA rejection due to its higher surface area (Table 2) and adsorption capacity (Supplementary Materials S2 and S3).

The long-term performance, i.e., rejection and water flux, of the kC-0.3%AC hydrogel was also investigated in three consecutive filtration cycles. Each filtration cycle lasted 1 h. The hydrogel was cleaned with DI water for 30 min at the end of each cycle before conducting the following filtration cycle with fresh wastewater. The results show decreased water flux and rejection of the kC-0.3%AC hydrogel in the consecutive filtration cycles. For example, the water flux in the kC-0.3% AC decreased slightly from 26.4 LMH in run 1 to 24.1 LMH in run 2 and 23 LMH in run 3. Besides, PFOA rejection decreased from 81.1% in run 1 to 75.1 in run 2 and 70.5% in run 3 (Fig. 6b). Understanding the equilibrium dynamics is crucial for optimizing PFOA removal at varying concentrations. Particle size or morphology changes can affect the hydrogel's ability to capture and retain contaminants, influencing its performance in consecutive filtration cycles. The PFOA-loaded kC-AC hydrogel consistently maintained its capacity for PFOA removal over three complete cycles. However, the decline in PFOA removal was noticeable in the second and third cycles. Adsorption tests confirm a decrease in the hydrogel's PFOA adsorption capacity in multiple filtration cycles. The decreased PFOA rejection may be attributed to the progressively diminished binding strength between PFOA and the hydrogel in the consecutive filtration cycles. The reduction in rejection efficiency likely arises from the saturation of adsorbent sites with adsorbate molecules after each cycle, resulting in fewer available sites for the adsorbate over time and consequently influencing the PFOA removal efficiency. The competition between PFOA and metal ions on the adsorption sites is another reason for the reduced hydrogel rejection

of PFOA in cycles 2 and 3 (Fig. 6b).

Furthermore, Fig. 6c and d shows that the kC-0.3%AC hydrogel removed the colour, 92% turbidity, 59% TDS, and 58% EC. Eliminating turbidity operates through the steric hindrance mechanism, wherein particles are excluded due to their size exceeding the hydrogel pore size, approximately 3.49 nm, as indicated in Table 2. In addition, the hydrogel has removed metal ions, for example, 76% Na, 90% K, 75% Si, 83% Cl, and 99% Al. AC's extensive surface area and porous structure facilitate efficient organic and inorganic adsorption. The kC-0.3%AC, incorporating ionizable groups from kC, selectively exchanges ions in applications like removing elements. The kC's diverse functional groups, including hydroxyl and sulphate, enhance element removal through electrostatic or chemical interactions. Concurrently, complexation contributes to the holistic capture and removal of specific elements from the solution, outlining the nuanced mechanisms underlying kC-AC hydrogel's targeted element removal.

Previous studies on the applicability of various hydrogels for PFAS wastewater treatment are listed in Table 3. V/AC-kC hydrogels have competitive performance with other hydrogels, with 79%–81% removal of PFOA from contaminated wastewater, knowing that the concentration of PFOA in this study was at least 1.8 times greater than those in Table 3. Also, this study used mixed wastewater from soil remediation containing metal ions such as silica, aluminium, and potassium in moderate concentrations. Also, V/AC-kC hydrogels are easy to fabricate at an affordable cost, about $ 1.5 per kilogram.

The kC-V and kC-AC hydrogels offer sustainable and environmentally friendly water and wastewater treatment methods. The hydrogel is made of natural and decomposable materials and does not require high energy for operation. Besides being gravity-driven, the kC-0.3%AC and kC-3%V hydrogel operate in a dead-end mode, leaving no wastewater/or brine solution behind, which is a problem in reverse osmosis and nanofiltration processes. Also, kC-0.3%AC performed better than kC-3% V hydrogel for PFOA removal from synthetic and actual wastewater.

5.7. Reusability of kC-AC and kC-V hydrogel

The reusability of adsorbents is crucial for mitigating waste production and reducing treatment costs. This study investigated the reusability of the kC-0.3%AC and kC-3%V hydrogels regarding % PFOA removal by repeating adsorption tests. Then, desorption experiments were carried out to assess the reversibility of the process and quantify the quantity of adsorbed PFOA in consecutive cycles. In the desorption procedure, methanol was introduced into vials containing 20 g of kC-0.3%AC-kC-3%V under monitor conditions. Subsequently, these isolated hydrogel specimens were suspended in methanol (MeOH), which can desorb PFOA from the hydrogel matrix. This method can be employed during regeneration processes, enabling the hydrogel's reutilization in successive cycles of PFOA adsorption.

In Fig. 7a and b, the percentage of PFOA removal in three cycles with kC-0.3%AC hydrogel was 82.8 ± 2 %,79.6 ± 2 %, and 77.9 ± 2 %, while in the kC-3%V was 81.5 % ± 2, 77.7% ± 2, and 74.8 % ± 2. The desorption concentration for the three cycles with kC-0.3%AC hydrogel was 77.8 ± 1 %, 70.9 ± 1%, and 67.7 ± 1 %. The corresponding PFOA desorption values for kC-3%V were 77.2 % ± 4,67.1 % ± 4, and 60.5 % ± 4.

Throughout the experimental procedure, it became evident that the PFOA-loaded kC-0.3%AC and kC-3%V hydrogels relatively maintained their capacity for PFOA removal over three complete adsorption-desorption cycles. A noticeable decline in removal efficiency was observed beyond the third cycle, attributed to the progressively diminished binding strength between PFOA and the hydrogel with each successive cycle. The reduction in adsorption efficiency likely arises from the saturation of adsorbent sites with adsorbate molecules after each cycle, resulting in fewer available sites for the adsorbate in subsequent cycles and, consequently, influencing the overall efficiency of the removal process. The capacity for successive adsorption-desorption cycles using the same adsorbent quantity, coupled with its effectiveness in removing PFOA from water, underscores the exceptional efficiency of the kC-AC- kC-V hydrogel as an adsorbent, suggesting a promising and potentially innovative and cost-effective approach for wastewater treatment.

5.8. Characterization of kC-AC and kC-V hydrogel after PFOA adsorption

SEM imaging enables a detailed assessment of kC-AC and kC-V hydrogel surface morphology after PFOA adsorption Fig. 7e and f. It has been observed that upon exposure to PFOA, the hydrogel's surface undergoes discernible changes manifested by surface roughening, formation of irregularities, or variations in surface topography. The nature and extent of these changes depend on factors such as PFOA concentration, exposure time, and the specific characteristics of the hydrogel material. Investigations indicated that PFOA can exhibit different distribution patterns, ranging from uniform coverage to localized clustering. The hydrogel's affinity for PFOA and the prevailing solution conditions may also influence the nature of the distribution. PFOA may preferentially adsorb in specific regions, forming aggregates or islands.

Table 3
Comparative analysis of PFAS removal efficiency by various hydrogel.

Type of Hydrogel	PFAS Type and Concentration	Type of Wastewater	Removal (%)	Reference
CTAB-functionalized alginate hydrogel	PFOA/50 mg/L	River water matrix	94.8 ± 2.1%	Naim Shaikh and Nawaz (2024)
Quaternized nanocellulose (QNC)	PFBA, PFBS, PFOA, & PFOS (N/A)	Contaminated groundwater	>95% for C7–C9 PFAS, 0% for PFBA, 10% for PFPeA	Li et al. (2023)
PEI-modified bio-adsorbents (PEI-BA, PEI-LF, PEI-PP)	PFOA/-	Synthetic water matrix	Up to 279.3 mg/g adsorption capacity	Qin et al. (2023)
Chitosan/F–COF	PFOS & PFOA/-	Lake water, sewage	Over 88.4% for three PFASs, maximum adsorption capacities: PFOS (8307.1 mg/g), PFOA (6177.1 mg/g), GenX (4603.3 mg/g)	He et al. (2022)
Chitosan-based hydrogel (CEGH)	PFOA/-	Synthetic water matrix	Maximum adsorption capacity: 1275.9 mg/g	Long et al. (2019)
CNC/PTMAEMA nanocomposite film	PFOA/(1, 10, and 100 mg/L)	Synthetic water matrix	61 %, 67 %, and 76 % respectively.	Gomri et al. (2023)
COF@CS composite gel	PFOA/-	Synthetic water matrix	Maximum adsorption capacity: 2.8 mmol/g	Zhang et al. (2024)
Acrylamide-based hydrogel composites with PAC	PFOS & PFOA (N/A)	Synthetic water matrix	98% for PFOS, 96% for PFOA	Klaus et al. (2023)
kappa carrageenan -Activated carbon	PFOA/(179.2 mg/L)	Soil-remediation wastewater	81.1%	This study
kappa carrageenan -vanillin	PFOA/(179.2 mg/L)	Soil-remediation wastewater	79.3%	This study

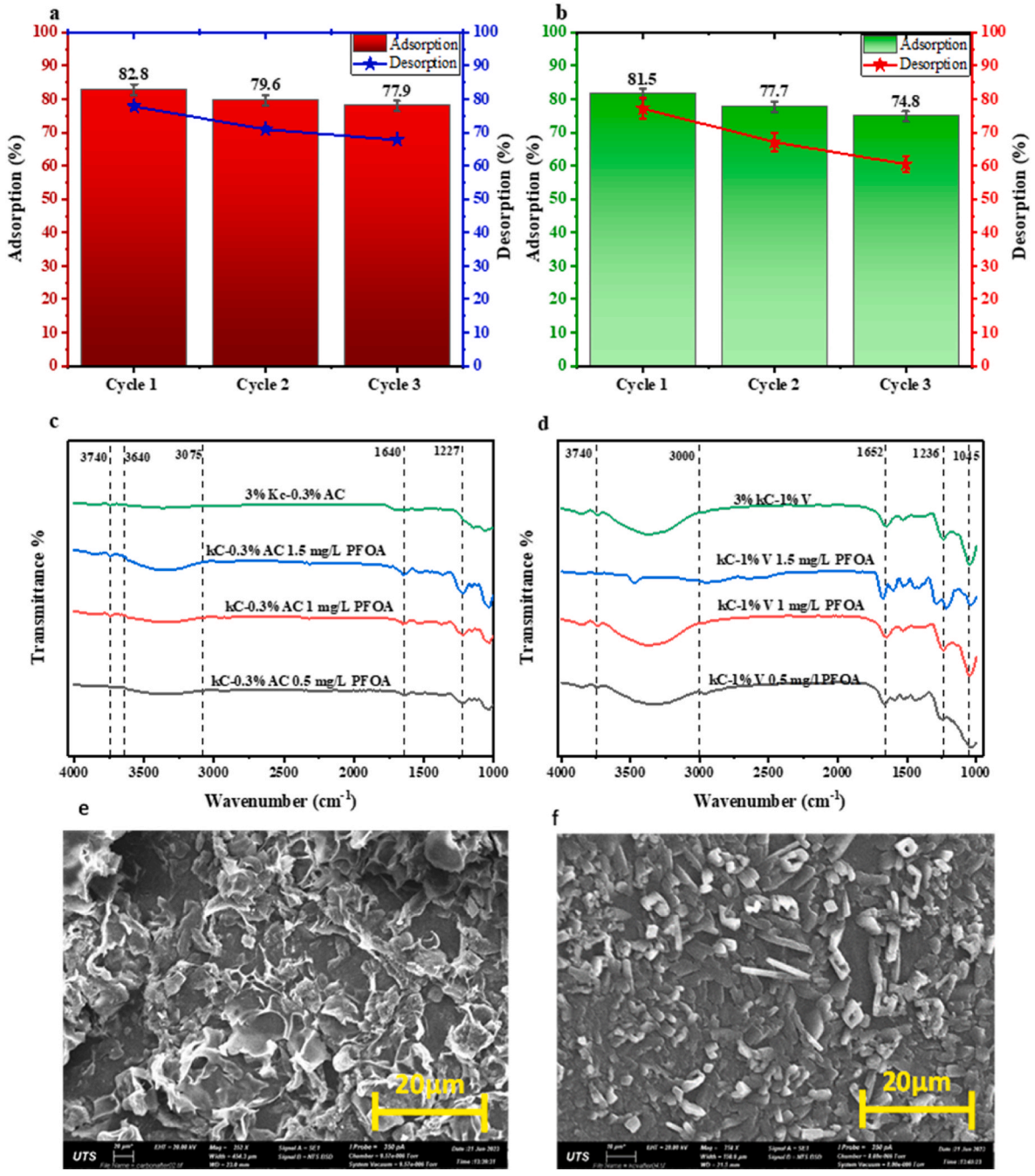

Fig. 7. a) adsorption and desorption of 1.5 mg/L PFOA in three consecutive cycles of 3%kC-0.3%AC, b) adsorption and desorption of PFOA in three consecutive cycles of 3%Kc-1%V, c) FT-IR of the different concentration AC (0.1,0.2,0.3)% with 3%kC after filtration, d) FT-IR of the different concentration V (1,2,3)% with 3% kC after filtration, e) SEM of the 3%kC-0.3%AC hydrogel after filtration at 20 μm at the first focus point, f) SEM of the 3%kC-3%V hydrogel after filtration at 20 μm at the first focus point. The error bar = 1 standard deviation.

These clusters' degree of aggregation and size can offer insights into the adsorption mechanism.

FTIR is a powerful tool for studying hydrogel and PFOA interactions. It detects shifts in absorption bands and signaling interactions between functional groups in the hydrogel and PFOA. New bands indicate the formation of chemical bonds. FTIR also confirms PFOA adsorption and offers insights into the adsorption mechanism, distinguishing between physical and chemical interactions. The FTIR spectra in Fig. 7c and d reveal discernible bands associated with different concentrations of PFOA (0.5, 1, and 1.5) mg/L, indicating its adsorption by the kC-0.3%AC and kC-3%V hydrogel. Notably, a peak at 1640 cm^{-1} in all kC-0.3%AC and kC-3%V hydrogel spectra post-adsorption indicates the deprotonated carboxylate group (COO^{-}) (Chen et al., 2017). Importantly, there is an escalation in the intensity of the 1640 cm^{-1} peak, mirroring the increase in the COO- concentration in the solution. This relationship underscores the role of attractions between the PFOA anion and the positively charged conjugate acid active sites on the kC-0.3%AC and kC-3%V surface as the principal driving force behind adsorption.

Additionally, the FTIR spectra in the 1000–1250 cm^{-1} capture the typical C–F bonds associated with PFOA. Various peaks at specific wavenumbers represent distinct features of the PFOA molecule, including the C–C bond at 1032 cm^{-1}, symmetric CF_2 stretches at 1227 cm^{-1}, asymmetric stretching of CF_2 and CF_3 at 1200-1240 cm-1, and another asymmetric CF_2 stretch (Gao and Chorover, 2012). As the pH

during adsorption increases, a noticeable reduction in the intensity of the C–F peaks on kC-0.3%AC and kC-3%V is observed. This effect can be attributed to decreased positively charged conjugate acid active sites on the kC-0.3%AC and kC-3%V surfaces, increasing repulsion between the negatively charged conjugate base active sites on kC-0.3%AC and kC-3% V and the PFOA anion.

EDS and EDX mapping analyses were conducted to characterize the nanoparticles and understand their distribution within the hydrogel cross-section. Figs. S5g, S5h, S5i, S5j, and Table S3 illustrate the EDS analysis of the section of the kC-0.3%AC and kC-3%V hydrogel after PFOA filtration. The results revealed the presence of carbon and oxygen in all membrane structures, indicating the composition of kC with either AC or vanillin (Figs. S5g, S5h, S5i, and S5j). Additionally, the detection of gold elements can be attributed to the surface deposition of gold during SEM imaging. Carbon, oxygen, sulphate, and a small amount of fluorine (0.03 wt%) were identified in the kC-0.3%AC and kC-3%V membrane structures. The EDS spectrum exhibited the highest intensities for fluorine and chloride ions, along with the presence of sodium, calcium, and sulfur as the primary constituents of the hydrogel after filtration. This finding suggests a relatively uniform distribution of elements within the membrane structure. After filtration, increased fluorine was observed in the hydrogel, 5.12 wt% and 4.04 wt% in the kC-0.3%AC and kC-3%V, respectively. Moreover, chloride was observed in the hydrogel, with concentrations of 2.24 wt% in kC-0.3%AC and 1.73 wt% in kC-3%V.

6. Conclusion

The study revealed kC-based hydrogel's exceptional efficiency in adsorbing various PFOA and pollutants, making it a compelling alternative for water purification. Incorporating vanillin and AC into the kC hydrogel significantly enhanced the kC-3%V membrane porosity, from 62.8% ± 5–79.1% ± 5 and up to 89.7% in the kC-0.3%AC. When evaluating the hydrogel's performance against PFOA, notable pH-dependent variations in rejection were observed. The hydrogel rejection of PFOA is pH-dependent, with the kC-0.3%AC hydrogel achieving an 86.9% rejection at pH 4, while the kC-3%V showed 85.7% rejection. Experiments also exhibited a decline in the water flux at higher PFOA concentrations and pH levels for both kC-0.3%AC and kC-3%V hydrogels. The study revealed that PFOA rejection increased with concentration, indicating that elevated PFOA levels restrict water passage by occupying pore spaces. When it was tested for soil remediation wastewater treatment, the kC-0.3%AC hydrogel removed 81.1% PFOA at 25.6 LMH water flux, while the kC-3%V hydrogel removed 79.3% PFOA at a water flux of 21.5 LMH. However, due to pore blocking, consecutive filtration cycles revealed a slight decline in the hydrogel's performance. More characterization results, such as pH at zero-point charge (pHpzc), X-ray diffraction (XRD), and X-ray photoelectron spectroscopy (XPS), should preferably be included in future work to understand the mechanisms of PFOA removal better.

CRediT authorship contribution statement

Lilyan Alsaka: Investigation, conceptualization, Data Analysis and curation, Validation, Writing –original draft, Writing – review and editing. **Ibrar Ibrar:** Investigation, Data Analysis and curation, writing. **Ali Altaee:** Supervision, Methodology, Conceptualization, Funding, Investigation, DataAnalysis and curation, Writing – review, and editing. **John Zhou:** Supervision, Data curation, Writing– review and editing. **Mahedy Hasan Chowdhury:** Data analysis, Data Curation. **Maryam AL-Ejji:** Investigation, Data analysis, Funding. **Alaa H. Hawari:** Data analysis, Funding, Writing – review and editing.

Declaration of competing interest

The authors declare that they have no known competing financial interests or personal relationships that could have appeared to influence the work reported in this paper.

Data availability

Data will be made available on request.

Acknowledgment

The authors gratefully acknowledge the financial support provided by Qatar National Research Fund research grant (MME03-1015-210003).

Appendix A. Supplementary data

Supplementary data to this article can be found online at https://doi.org/10.1016/j.chemosphere.2024.143371.

References

Alam, J., Alhoshan, M., Shukla, A.K., Aldalbahi, A., Ali, F.A.A., 2019. k-Carrageenan – a versatile biopolymer for the preparation of a hydrophilic PVDF composite membrane. Eur. Polym. J. 120, 109219. https://doi.org/10.1016/j.eurpolymj.2019.109219.

Alam, J., Alhoshan, M., Shukla, A.K., Aldalbahi, A., Ali, F.A.A., Dass, L.A., Muthumareeswaran, M.R., 2017. κ-Carrageenan as a promising pore-former for the preparation of a highly porous polyphenylsulfone membrane. Mater. Lett. 204, 108–111. https://doi.org/10.1016/j.matlet.2017.06.017.

Alsalhy, Q.F., Rashid, K.T., Ibrahim, S.S., Ghanim, A.H., Van der Bruggen, B., Luis, P., Zablouk, M., 2013. Poly(vinylidene fluoride-co-hexafluoropropylene) (PVDF-co-HFP) hollow fiber membranes prepared from PVDF-co-HFP/PEG-600Mw/DMAC solution for membrane distillation. J. Appl. Polym. Sci. 129 (6), 3304–3313. https://doi.org/10.1002/app.39065.

AlSawaftah, N., Abuwatfa, W., Darwish, N., Husseini, G., 2021. A comprehensive review on membrane fouling: mathematical modelling, prediction, diagnosis, and mitigation. Water (Basel) 13 (9), 1327. https://doi.org/10.3390/w13091327.

Appleman, T.D., Higgins, C.P., Quiñones, O., Vanderford, B.J., Kolstad, C., Zeigler-Holady, J.C., Dickenson, E.R.V., 2014. Treatment of poly- and perfluoroalkyl substances in U.S. full-scale water treatment systems. Water Res. 51, 246–255. https://doi.org/10.1016/j.watres.2013.10.067.

Arthanareeswaran, G., Thanikaivelan, P., Raajenthiren, M., 2009. Preparation and characterization of poly (methyl methacrylate) and sulfonated poly (ether ether ketone) blend ultrafiltration membranes for protein separation applications. Mater. Sci. Eng. C 29 (1), 246–252. https://doi.org/10.1016/j.msec.2008.06.015.

Ateia, M., Alsbaiee, A., Karanfil, T., Dichtel, W., 2019. Efficient PFAS removal by amine-functionalized sorbents: critical review of the current literature. Environ. Sci. Technol. Lett. 6 (12), 688–695. https://doi.org/10.1021/acs.estlett.9b00659.

Balasubramanian, R., Kim, S.S., Lee, J., 2018. Novel synergistic transparent k-Carrageenan/Xanthan gum/Gellan gum hydrogel film: mechanical, thermal and water barrier properties. Int. J. Biol. Macromol. 118 (Pt A), 561–568. https://doi.org/10.1016/j.ijbiomac.2018.06.110.

Bhushan, B., Yong Chae, J., 2011. Natural and biomimetic artificial surfaces for superhydrophobicity, self-cleaning, low adhesion, and drag reduction. Prog. Mater. Sci. 56 (1), 1–108. https://doi.org/10.1016/j.pmatsci.2010.04.003.

Buck, R.C., Franklin, J., Berger, U., Conder, J.M., Cousins, I.T., De Voogt, P., Jensen, A. A., Kannan, K., Mabury, S.A., van Leeuwen, S.P., 2011. Perfluoroalkyl and polyfluoroalkyl substances in the environment: terminology, classification, and origins. Integrated Environ. Assess. Manag. 7 (4), 513–541.

Chen, W., Zhang, X., Mamadiev, M., Wang, Z., 2017. Sorption of perfluorooctane sulfonate and perfluorooctanoate on polyacrylonitrile fiber-derived activated carbon fibers: in comparison with activated carbon. RSC advances 7 (2), 927–938. https://doi.org/10.1039/C6RA25230C.

Das, S., Ronen, A., 2022. A review on removal and destruction of per- and polyfluoroalkyl substances (PFAS) by novel membranes. Membranes 12 (7), 662. https://doi.org/10.3390/membranes12070662.

Eke, J., Banks, L., Mottaleb, M.A., Morris, A.J., Tsyusko, O.V., Escobar, I.C., 2020. Dual-functional phosphorene nanocomposite membranes for the treatment of perfluorinated water: an investigation of perfluorooctanoic acid removal via filtration combined with ultraviolet irradiation or oxygenation. Membranes 11 (1), 18. https://doi.org/10.3390/membranes11010018.

Esmaeili, M., Lahti, J., Virtanen, T., Mänttäri, M., Kallioinen, M., 2020. The interplay role of vanillin, water, and coagulation bath temperature on formation of antifouling polyethersulfone (PES) membranes: application in wood extract treatment. Separ. Purif. Technol. 235, 116225.

Flores, C., Ventura, F., Martin-Alonso, J., Caixach, J., 2013. Occurrence of perfluorooctane sulfonate (PFOS) and perfluorooctanoate (PFOA) in N.E. Spanish surface waters and their removal in a drinking water treatment plant that combines conventional and advanced treatments in parallel lines. Sci. Total Environ. 461–462, 618–626. https://doi.org/10.1016/j.scitotenv.2013.05.026.

Franke, V., McCleaf, P., Lindegren, K., Ahrens, L., 2019. Efficient removal of per-and polyfluoroalkyl substances (PFASs) in drinking water treatment: nanofiltration combined with active carbon or anion exchange. Environmental Science: Water Research & Technology 5 (11), 1836–1843.

Gao, X., Chorover, J., 2012. Adsorption of perfluorooctanoic acid and perfluorooctanesulfonic acid to iron oxide surfaces as studied by flow-through ATR-FTIR spectroscopy. Environ. Chem. 9 (2), 148. https://doi.org/10.1071/EN11119.

Gomri, C., Benkhaled, B.T., Chaix, A., Dorandeu, C., Chopineau, J., Petit, E., Aissou, K., Cot, D., Cretin, M., Semsarilar, M., 2023. A facile approach to modify cellulose nanocrystal for the adsorption of perfluorooctanoic acid. Carbohydr. Polym. 319, 121189.

Hamid, M.F., Abdullah, N., Yusof, N., Lau, W.J., Ismail, A.F., Wan Salleh, W.N., Jaafar, J., Aziz, F., 2021. Innovative polymer-complex draw solution for copper(II) removal using forward osmosis. J. Environ. Chem. Eng. 9 (1), 104854. https://doi.org/10.1016/j.jece.2020.104854.

Hamidi, M., Azadi, A., Rafiei, P., 2008. Hydrogel nanoparticles in drug delivery. Adv. Drug Deliv. Rev. 60 (15), 1638–1649.

He, C., Yang, Y., Hou, Y.-J., Luan, T., Deng, J., 2022. Chitosan-coated fluoro-functionalized covalent organic framework as adsorbent for efficient removal of per-and polyfluoroalkyl substances from water. Separ. Purif. Technol. 294, 121195.

Ibrar, I., Alsaka, L., Yadav, S., Altaee, A., Zhou, J.L., Shon, H.K., 2023. Kappa carrageenan-vanillin composite hydrogel for landfill leachate wastewater treatment. Desalination 565, 116826. https://doi.org/10.1016/j.desal.2023.116826.

Jin, T., Peydayesh, M., Joerss, H., Zhou, J., Bolisetty, S., Mezzenga, R., 2021. Amyloid fibril-based membranes for PFAS removal from water. Environmental science water research & technology 7 (1), 1873–1884. https://doi.org/10.1039/d1ew00373a.

Klaus, M.V.X., Gutierrez, A.M., Hilt, J.Z., 2023. Development of poly (acrylamide)-Based hydrogel composites with powdered activated carbon for controlled sorption of PFOA and PFOS in aqueous systems. Polymers 15 (22), 4384.

Kostov, K.G., Nishime, T.M.C., Castro, A.H.R., Toth, A., Hein, L.R.O., 2014. Surface modification of polymeric materials by cold atmospheric plasma jet. Appl. Surf. Sci. 314, 367–375. https://doi.org/10.1016/j.apsusc.2014.07.009.

Kumarasamy, E., Manning, I.M., Collins, L.B., Coronell, O., Leibfarth, F.A., 2020. Ionic fluorogels for remediation of per- and polyfluorinated alkyl substances from water. ACS Cent. Sci. 6 (4), 487–492. https://doi.org/10.1021/acscentsci.9b01224.

Lei, X., 2023. Perfluorooctanoic acid (PFOA) adsorption by ordered mesoporous carbon (OMC) and polyethyleneimine modified graphene oxide (GO-PEI). Effects of Water Matrices and Understanding Mechanisms. University of Louisiana at Lafayette.

Li, D., Lee, C.-S., Zhang, Y., Das, R., Akter, F., Venkatesan, A.K., Hsiao, B.S., 2023. Efficient removal of short-chain and long-chain PFAS by cationic nanocellulose. J. Mater. Chem. A 11 (18), 9868–9883.

Liu, S., Li, L., 2016. Recoverable and self-healing double network hydrogel based on κ-carrageenan. ACS Appl. Mater. Interfaces 8 (43), 29749–29758. https://doi.org/10.1021/acsami.6b11363.

Long, L., Hu, X., Yan, J., Zeng, Y., Zhang, J., Xue, Y., 2019. Novel chitosan–ethylene glycol hydrogel for the removal of aqueous perfluorooctanoic acid. J. Environ. Sci. 84, 21–28.

Mahdavinia, G.R., Bazmizeynabad, F., Seyyedi, B., 2015. kappa-Carrageenan beads as new adsorbent to remove crystal violet dye from water: adsorption kinetics and isotherm. Desalination Water Treat. 53 (9), 2529–2539.

Milley, S.A., Koch, I., Fortin, P., Archer, J., Reynolds, D., Weber, K.P., 2018. Estimating the number of airports potentially contaminated with perfluoroalkyl and polyfluoroalkyl substances from aqueous film forming foam: a Canadian example. J. Environ. Manag. 222, 122–131.

Naim Shaikh, M.A., Nawaz, T., 2024. Highly efficient cationic surfactant functionalized alginate hydrogel for perfluorooctanoic acid adsorption: optimization through response surface methodology and performance evaluation for aqueous media. ACS ES&T Water 4 (7), 3078–3088.

Ouyang, Z., Huang, Z., Tang, X., Xiong, C., Tang, M., Lu, Y., 2019. A dually charged nanofiltration membrane by pH-responsive polydopamine for pharmaceuticals and personal care products removal. Separ. Purif. Technol. 211, 90–97. https://doi.org/10.1016/j.seppur.2018.09.059.

Pensini, E., Dinardo, A., Lamont, K., Longstaffe, J., Elsayed, A., Singh, A., 2019. Effect of salts and pH on the removal of perfluorooctanoic acid (PFOA) from aqueous solutions through precipitation and electroflocculation. Can. J. Civ. Eng. 46 (10), 881–886. https://doi.org/10.1139/cjce-2018-0705.

Qin, F., Yao, W., Liu, Y., Zhu, B., Yang, Q., Zheng, Y., 2023. Polyethyleneimine functionalized cellulose-rich agroforestry residues for removing perfluorooctanoic acid: adsorption performance and mechanism. Cellulose 30 (6), 3653–3666.

R, S.K., G, A., Y, L.T., A F, I., 2017. Enhancement of permeability and antibiofouling properties of polyethersulfone (PES) membrane through incorporation of quorum sensing inhibition (QSI) compound. J. Taiwan Inst. Chem. Eng. 72, 200–212. https://doi.org/10.1016/j.jtice.2017.01.012.

Tang, C.Y., Fu, Q.S., Robertson, A.P., Criddle, C.S., Leckie, J.O., 2006. Use of reverse osmosis membranes to remove perfluorooctane sulfonate (PFOS) from semiconductor wastewater. Environ. Sci. Technol. 40 (23), 7343–7349. https://doi.org/10.1021/es060831q.

Xu, J., Liu, J., Ling, P., Zhang, X., Xu, K., He, L., Wang, Y., Su, S., Hu, S., Xiang, J., 2020. Raman spectroscopy of biochar from the pyrolysis of three typical Chinese biomasses: a novel method for rapidly evaluating the biochar property. Energy 202, 117644.

Yadav, S., Ibrar, I., Samal, A.K., Altaee, A., Déon, S., Zhou, J., Ghaffour, N., 2022. Preparation of fouling resistant and highly perm-selective novel PSf/GO-vanillin nanofiltration membrane for efficient water purification. J. Hazard Mater. 421. https://doi.org/10.1016/j.jhazmat.2021.126744, 126744-126744.

Yang, B., Yang, X., Liu, B., Chen, Z., Chen, C., Liang, S., Chu, L.-Y., Crittenden, J., 2017. PVDF blended PVDF-g-PMAA pH-responsive membrane: effect of additives and solvents on membrane properties and performance. J. Membr. Sci. 541, 558–566. https://doi.org/10.1016/j.memsci.2017.07.045.

Yu, Q., Deng, S., Yu, G., 2008. Selective removal of perfluorooctane sulfonate from aqueous solution using chitosan-based molecularly imprinted polymer adsorbents. Water Res. 42 (12), 3089–3097. https://doi.org/10.1016/j.watres.2008.02.024.

Zeng, C., Tanaka, S., Suzuki, Y., Fujii, S., 2017a. Impact of feed water pH and membrane material on nanofiltration of perfluorohexanoic acid in aqueous solution. Chemosphere 183, 599–604.

Zeng, C., Tanaka, S., Suzuki, Y., Fujii, S., 2017b. Impact of feed water pH and membrane material on nanofiltration of perfluorohexanoic acid in aqueous solution. Chemosphere 183, 599–604. https://doi.org/10.1016/j.chemosphere.2017.05.132.

Zeng, C., Tanaka, S., Suzuki, Y., Yukioka, S., Fujii, S., 2017c. Rejection of trace level perfluorohexanoic acid (PFHxA) in pure water by loose nanofiltration membrane. J. Water Environ. Technol. 15 (3), 120–127. https://doi.org/10.2965/jwet.16-072.

Zhang, Q., Deng, S., Yu, G., Huang, J., 2011. Removal of perfluorooctane sulfonate from aqueous solution by crosslinked chitosan beads: sorption kinetics and uptake mechanism. Bioresour. Technol. 102 (3), 2265–2271. https://doi.org/10.1016/j.biortech.2010.10.040.

Zhang, X., He, A., Guo, R., Zhao, Y., Yang, L., Morita, S., Xu, Y., Noda, I., Ozaki, Y., 2022. A new approach to removing interference of moisture from FTIR spectrum. Spectrochimica acta. Part A, Molecular and biomolecular spectroscopy 265, 120373. https://doi.org/10.1016/j.saa.2021.120373.

Zhang, X., Wang, S., Zhu, X., Zhu, D., Wang, W., Wang, B., Deng, S., Yu, G., 2024. Efficient removal of per/polyfluoroalkyl substances from water using recyclable chitosan-coated covalent organic frameworks: experimental and theoretical methods. Chemosphere 356, 141942.

Zhao, C., Nie, S., Tang, M., Sun, S., 2011. Polymeric pH-sensitive membranes—a review. Prog. Polym. Sci. 36 (11), 1499–1520. https://doi.org/10.1016/j.progpolymsci.2011.05.004.

Zheng, B., Liu, X., Guo, R., Fu, Q., Zhao, X., Wang, S., Chang, S., Wang, X., Geng, M., Yang, G., 2017. Distribution characteristics of poly-and perfluoroalkyl substances in the Yangtze River Delta. J. Environ. Sci. 61 (11), 97–109. https://doi.org/10.1016/j.jes.2017.09.015.

Zhou, J., Saeidi, N., Wick, L.Y., Kopinke, F.-D., Georgi, A., 2021. Adsorption of polar and ionic organic compounds on activated carbon: surface chemistry matters. Sci. Total Environ. 794. https://doi.org/10.1016/j.scitotenv.2021.148508, 148508-148508.

Zhu, Y., Tang, J., Li, M., Wang, H., Yang, H., 2021. Contamination status of perfluorinated compounds and its combined effects with organic PollZutants. Asian J. Ecotoxicol. 16, 86–99.